ARTICLE
Journal of Cellular Biochemistry 114:2415–2429 (2013)

Journal of Cellular Biochemistry

Formation of Cofilin–Actin Rods Following Cucurbitacin-B-Induced Actin Aggregation Depends on Slingshot Homolog 1-Mediated Cofilin Hyperactivation

Yan-Ting Zhang,[1] Dong-Yun Ouyang,[1] Li-Hui Xu,[1,2] Qing-Bing Zha,[1] and Xian-Hui He[1]*

[1]*Department of Immunobiology, Jinan University, Guangzhou, 510632, China*

[2]*Department of Cell Biology, Jinan University, Guangzhou, 510632, China*

ABSTRACT

Accumulating evidence indicates that cucurbitacin B (CuB), as well as other cucurbitacins, damages the actin cytoskeleton in a variety of cell types. However, the underlying mechanism of such an effect is not well understood. In this study, we showed that CuB rapidly induced actin aggregation followed by actin rod formation in melanoma cells. Cofilin, a critical regulator of actin dynamics, was dramatically dephosphorylated (i.e., activated) upon CuB treatment. Notably, the activated cofilin subsequently formed rod-like aggregates, which were highly colocalized with actin rods, indicating the formation of cofilin–actin rods. Cofilin knockdown significantly suppressed rod formation but did not prevent actin aggregation. Furthermore, knockdown of the cofilin phosphatase Slingshot homolog 1 (SSH1), but not chronophin (CIN), alleviated CuB-induced cofilin hyperactivation and cofilin–actin rod formation. The activity of Rho kinase and LIM kinase, two upstream regulators of cofilin activation, was downregulated after cofilin hyperactivation. Pretreatment with a thiol-containing reactive oxygen species (ROS) scavenger *N*-acetyl cysteine, but not other ROS inhibitors without thiol groups, suppressed CuB-induced actin aggregation, cofilin hyperactivation and cofilin–actin rod formation, suggesting that thiol oxidation might be involved in these processes. Taken together, our results demonstrated that CuB-induced formation of cofilin–actin rods was mediated by SSH1-dependent but CIN-independent cofilin hyperactivation. J. Cell. Biochem. 114: 2415–2429, 2013.

KEY WORDS: CUCURBITACIN B; MELANOMA; ACTIN AGGREGATION; COFILIN; COFILIN–ACTIN RODS; SLINGSHOT HOMOLOG 1

Cucurbitacins belong to a large family of triterpenoid compounds isolated from *Cucurbitaceae* plants, which have been used as folk medicines for centuries [Jayaprakasam et al., 2003; Chen et al., 2012]. Several members of cucurbitacins, such as cucurbitacin B (CuB), E, and I, have been shown to exhibit a wide range of biological activities, including anticancer, hepatoprotective, and anti-inflammatory effects [Jayaprakasam et al., 2003; Chen et al., 2005]. Their anticancer mechanisms have been investigated in a variety of tumor cell lines as well as normal cells [Chen et al., 2005, 2012]. Emerging evidence indicates that cucurbitacins rapidly disrupt the actin cytoskeleton in different cell types, leading to a reduction in globular actin (G-actin) pool and the formation of actin aggregates [Duncan et al., 1996; Haritunians et al., 2008; Yin et al., 2008; Knecht et al., 2010; Boykin et al., 2011; Zhang et al., 2011]. Consequently, the morphology of cells is quickly impaired, and the cell motility and cytokinesis are also suppressed [Knecht et al., 2010; Zhang et al., 2011].

Several recent studies shed new light on the action mechanism of cucurbitacins. One study revealed that cucurbitacin I inhibits cell motility by indirectly interfering with actin dynamics [Knecht et al., 2010]. Another study indicated that cucurbitacin E and I induce cofilin dephosphorylation (activation) in leukemia cells [Nakashima et al., 2010]. However, cucurbitacins E and I, which disrupt the actin cytoskeleton and dephosphorylate cofilin in mammalian cells, do not induce actin polymerization in *Dictyostelium* and in purified actin [Momma et al., 2008; Knecht et al., 2010].

The authors declare that they have no conflict of interest.

Yan-Ting Zhang and Dong-Yun Ouyang contributed equally to this work.

Grant sponsor: National Natural Science Foundation of China; Grant number: 81173604; Grant sponsor: Specialized Research Program of "Twelfth Five-Year Plan" of China; Grant number: 2011ZX09307-303-03; Grant sponsor: Fundamental Research Funds for the Central Universities; Grant number: 21611387.

*Correspondence to: Dr. Xian-Hui He, Department of Immunobiology, Jinan University, Guangzhou 510632, P.R. China. E-mail: thexh@jnu.edu.cn

Manuscript Received: 25 April 2012; Manuscript Accepted: 2 May 2013

Accepted manuscript online in Wiley Online Library (wileyonlinelibrary.com): 20 May 2013

DOI 10.1002/jcb.24587 • © 2013 Wiley Periodicals, Inc.

Thus, the mechanism underlying the cucurbitacin-induced disruption of actin cytoskeleton is not fully understood. Specifically, it is unclear how the cofilin is dephosphorylated by cucurbitacins and what the role of cofilin activation is in actin aggregation.

Cofilin, an actin-depolymerizing factor, is a critical regulator of actin dynamics that is regulated by a large number of factors, such as phosphatidylinositol phosphate (PtdIns(3)P) and bis-phosphate (PtdIns(3,4)P2), pH, oxidation, and competition with tropomyosins [DesMarais et al., 2005; Bamburg and Bernstein, 2010; Zdanov et al., 2010]. In metazoans, cofilin can sever actin filaments (F-actin) when it is activated through dephosphorylation at the conserved serine residue 3 by Slingshot phosphatases (SSH), chronophin (CIN) or other phosphatases, whereas it is inactivated by phosphorylation via LIM kinases (LIMKs) or TES kinases (TESKs) [Meberg et al., 1998; Niwa et al., 2002; Wang et al., 2007]. Rho GTPase and its downstream effector Rho-associated kinase (ROCK) also regulate the activity of cofilin, thus modulating the stress fibers and focal adhesions [Van Troys et al., 2008]. ROCK does not phosphorylate cofilin directly but phosphorylates LIMKs, which in turn inactivate cofilin [Jang et al., 2005]. The ROCK/LIMK/cofilin pathway has been shown to modulate actin assembly in a variety of cell types in response to various extracellular stimuli [Lin et al., 2003]. Given the critical role of cofilin in modulating the actin cytoskeleton, further studies on the involvement of cofilin in cucurbitacin-induced actin aggregation in cells are warranted.

We have previously shown that CuB induces a depletion of G-actin pool in B16F10 cells [Zhang et al., 2011]. In this study, we further observed that cofilin was hyperactivated and then reorganized into cofilin–actin rods following the formation of actin aggregates in both CuB-treated A375 and B16F10 melanoma cells. Knockdown of cofilin or its upstream phosphatase Slingshot homolog 1 (SSH1), instead of CIN, significantly suppressed the formation of cofilin–actin rods. However, actin aggregation was not alleviated upon cofilin or SSH1 knockdown. Our results suggested that CuB-induced cofilin–actin rod formation was a downstream event of actin aggregation, and was likely mediated by SSH1-dependent cofilin hyperactivation.

MATERIALS AND METHODS

CHEMICALS AND REAGENTS

CuB (molecular weight 558.7 Da) with 98% purity was obtained from Zhongxin Innova Laboratories (Tianjin, China), dissolved in dimethyl sulfoxide (DMSO) at 10 mM, and stored at −20°C. Triton X-100, sucrose, sodium deoxycholate, *N*-acetyl-L-cysteine (NAC), dithiothreitol (DTT), propidium iodide, paraformaldehyde, diphenyleneiodonium chloride (DPI) and VAS2870 (VAS) and DMSO were from Sigma–Aldrich (St Louis, MO). RNase A was purchased from Invitrogen (Carlsbad, CA).

CELL CULTURE

Human A375 and murine B16F10 melanoma cell lines were obtained from the Cell Bank of the Chinese Academy of Sciences (Shanghai, China). Cells were cultured in DMEM (Invitrogen) supplemented with 10% fetal bovine serum (FBS; Invitrogen), 100 U/ml penicillin, and 100 μg/ml streptomycin (Invitrogen), and maintained at 37°C in a humidified incubator of 5% CO_2.

CELL PROLIFERATION ASSAY

Cell proliferation was measured by MTS assay using the CellTiter 96 Aqueous ONE Solution kit (Promega, Madison, WI). The modified MTS assay is often described as a "one-step" MTT assay, which offers the convenience of adding the reagent straight to cell culture without intermittent steps required in the conventional MTT assay. Briefly, cells were seeded into 96-well plates at a density of 4×10^4/ml and 100 μl/well for 24 h. On the next day, culture medium was replaced with fresh one containing indicated concentrations of CuB or vehicle (DMSO). After incubation for additional 48 h, MTS reagent (20 μl) was added to each well and incubated at 37°C for 1–4 h. The absorbance at 490 nm was measured using a microplate reader (Model 680; Bio-Rad, Richmond, CA). Three independent experiments were performed, each in triplicates.

IMMUNOFLUORESCENCE MICROSCOPY

After incubation with CuB, cells were fixed in 4% paraformaldehyde prepared in phosphate-buffered saline (PBS), permeabilized with ice-cold 100% methanol, and immunostained with mouse anti-β-actin and rabbit anti-β-tubulin or rabbit anti-cofilin antibodies (Cell Signaling Technology, Danvers, MA) or rabbit anti-SSH1 (Abcam, Hong Kong), followed by CF488-conjugated goat-anti-mouse IgG or CF568-conjugated goat-anti-rabbit IgG, highly cross-absorbed (Biotium, Hayward, CA). Nuclei were revealed by Hoechst33342 staining. Fluorescence images were observed and collected under a Leica DMIRB fluorescent microscope (Leica Microsystems, Wetzlar, Germany) armed with a Spinning Disk Confocal Microscopy system (UltraView cooled CCD; Perkin Elmer, Waltham, MA).

COLOCALIZATION ANALYSIS

All fluorescence image analysis was conducted using ImageJ software (National Institutes of Health, Bethesda, MD). Colocalization analysis was performed using Intensity Correlation Analysis (ICA) method as described previously [Li et al., 2004]. The PDM value is the Product of the Differences from the Mean, that is, for each pixel: PDM = (red intensity − mean red intensity × (green intensity − mean green intensity). PDM images were created using a plugin for ImageJ found at http://www.uhnresearch.ca/facilities/wcif/imagej/colour_analysis.htm#coloc_coeff. ICA produces a PDM image of graded colocalization, where positive PDM value correspond to a high degree of colocalization (here maximum values shown in yellow), zero values to random distribution (here: black) and negative values to mutual exclusion of labels (here minimum values shown in blue). In each PDM image, a PDM scale bar is inserted. Moreover, the Intensity Correlation Quotient (ICQ) values are shown in quantitative colocalization analysis. The ICQ is equal to the ratio of the number of positive PDM values to the total number of pixel values. From this ratio, 0.5 is subtracted to yield ICQ values distributed between −0.5 and +0.5 where random colocalization gives an ICQ of ∼0, segregated or asynchronous colocalization gives $0 > \text{ICQ} \geq -0.5$, and dependent or synchronous colocalization yields $0 < \text{ICQ} \leq +0.5$.

CELL CYCLE ANALYSIS

Analysis of cell cycle was performed as described previously [Zhang et al., 2011]. In brief, cells were fixed and stained with PBS containing 50 μg/ml propidium iodide (PI) and 30 μg/ml of RNase A. DNA

content data were acquired using CELLQuest software on a flow cytometer (FACSCalibur; Becton Dickinson, Mountain View, CA) and analyzed using ModFit LT (Verity, Topsham, ME).

CELL MIGRATION ASSAY

Cell migration ability was determined by Scratch wound-healing assay as previously described [Zhang et al., 2011]. Migrated cells were observed by microscopy and photographed at 0, 24, and 48 h from addition of indicated drugs. The wound widths in terms of pixels were quantitated with PhotoShop V8.0 (Adobe, San Jose, CA).

EXTRACTION OF SOLUBLE ACTIN

Soluble actin (referred as G-actin hereafter) was extracted as described previously [Zhang et al., 2011]. Briefly, cells were washed twice with cold PBS (4°C) after exposure to CuB or vehicle (control) for indicated time lengths. G-actin was extracted with soluble actin extraction solution (containing 0.2% Triton X-100) from the cells. The residues were lysed using 2× loading buffer for sodium dodecyl sulfate–polyacrylamide gel electrophoresis (SDS–PAGE).

WESTERN BLOT ANALYSIS

Samples were prepared as described above or by lysing PBS-washed cells with RIPA buffer (Beyotime, Haimen, China). The proteins were separated by SDS–PAGE followed by electro-transfer to polyvinylidene difluoride membrane (Hybond-P; GE Healthcare Life Sciences, Piscataway, NJ). The membrane was probed using antibodies against phospho-cofilin, cofilin, CIN, phospho-LIMK1/2, LIMK2, ROCK1, β-tubulin (Cell Signaling Technology), SSH1 (Abcam), and pan-actin (Santa Cruz Biotechnology, Santa Cruz, CA), followed by a horseradish peroxidase (HRP)-conjugated second antibody (1:10,000; Jackson ImmunoResearch, West Grove, PA). Bands were revealed with enhanced chemiluminescence kit (BeyoECL Plus; Beyotime) and recorded on X-ray films (Kodak; Xiamen, Fujian, China). The densitometry of each band was quantified by FluorChem 8000 (AlphaInnotech, San Leandro, CA).

RNA INTERFERENCE ASSAY

The siRNA duplexes (#6267) targeting cofilin was obtained from Cell Signaling Technology. The siRNA (5′-CCGACAUCCUCUUUGGC-CAdTdT-3′) duplexes targeting CIN and negative control siRNA were designed and synthesized by Sigma–Aldrich. The siRNA (5′-CGGAGAACCUAAACAACAAdTdT-3′) duplexes targeting SSH1 were designed and synthesized by RiboBio (Guangzhou, China). Transfection was performed using N-TER Nanoparticle siRNA Transfection System (Sigma–Aldrich) according to the manufacturer's protocol. In brief, 1×10^4 A375 cells were plated in 35-mm dishes and cultured overnight. Cofilin (40 nM), CIN (20 nM), SSH1 (20 nM), and negative control siRNA (20 nM) were transfected into cells, respectively. After 72 h incubation at 37°C, the silencing efficiency was determined by Western blot using specific antibodies. After knockdown for 72 h, the effect of CuB on cofilin dephosphorylation and actin cytoskeleton were measured by Western blot and immunofluorescence microscopy.

ANALYSIS OF ROS PRODUCTION

ROS levels within cells were determined by flow cytometry or fluorescence microscopy using H_2DCF-DA (Molecular Probes, Eugene, USA), an ROS-sensitive fluorescent compound that can readily diffuse into cells and be hydrolyzed by intracellular esterase to form H_2DCF within cells. The latter is then oxidized by ROS, if there were, to produce fluorescent compound dichlorofluorescein (DCF). In this study, we first stained A375 cells with H_2DCF-DA (10 μM) for 30 min, and then treated the cells with CuB for 30 min. Then ROS levels in cells were analyzed.

STATISTICAL ANALYSIS

Unless otherwise indicated, all experiments were performed in triplicate, with one representative experiment shown. Data were expressed as mean ± SD. Statistical analysis was performed using GraphPad Prism 4.0 (GraphPad Software, Inc., San Diego, CA). One-way ANOVA, followed by Dunnett's multiple comparison tests, was used to analyze the statistical significance among multiple groups. P values <0.05 were considered statistically significant.

RESULTS

CUCURBITACIN B INDUCED ACTIN AGGREGATION FOLLOWED BY ROD-LIKE ACTIN STRUCTURES IN MELANOMA CELLS

Previously, we have demonstrated that the G-actin pool is quickly depleted through actin aggregation, but afterwards partly restored, by CuB treatment in B16F10 cells [Zhang et al., 2011]. Similarly, CuB induced actin aggregation and G-actin depletion, which were correlated with cell growth inhibition, in other cell lines including in HeLa (data not shown) and A375 cells (Fig. 1, Supplementary Figs. S1 and S2). To explore the mechanism underlying such an action of CuB, we first observed the change of cytoskeleton structures in both A375 and B16F10 cells after exposure to CuB. Immunofluorescence microscopy showed that CuB treatment induced marked actin aggregation in melanoma cells (Fig. 1 and Supplementary Fig. S3). During the first few hours, both the number and size of amorphous actin aggregates were gradually increased, meanwhile the cortical actin filaments were destructed. These observations were supported by Western blot analysis of the cellular actin levels (Supplementary Fig. S2), suggesting that the depleted G-actin pool and the disappeared cortical F-actin filaments had been converted into actin aggregates. Interestingly, rod-like actin structures emerged following the actin aggregation. After 4 h of CuB exposure, actin rods became the main form of actin aggregation, although there were still amorphous actin aggregates in the cells. After 24 h of CuB incubation, the amount of actin rods was gradually reduced as compared with that of 4 h. These rods seemed reversible since they disappeared 20 h after removal of CuB from the culture medium, whereas some amorphous actin aggregates were retained (Fig. 1). Unlike the actin filaments, the microtubules seemed unaffected by CuB treatment, and were not colocalized with the actin aggregates in both A375 and B16F10 cells (Fig. 1 and Supplementary Fig. S3). These results suggested that G-actin depletion was due to rapid actin aggregation followed by actin rod formation in CuB-treated cells.

CUCURBITACIN B INDUCED COFILIN HYPERACTIVATION AND COFILIN–ACTIN ROD FORMATION

Cofilin is a critical regulator of actin dynamics, which has F-actin severing activity after dephosphorylation (activation) [DesMarais

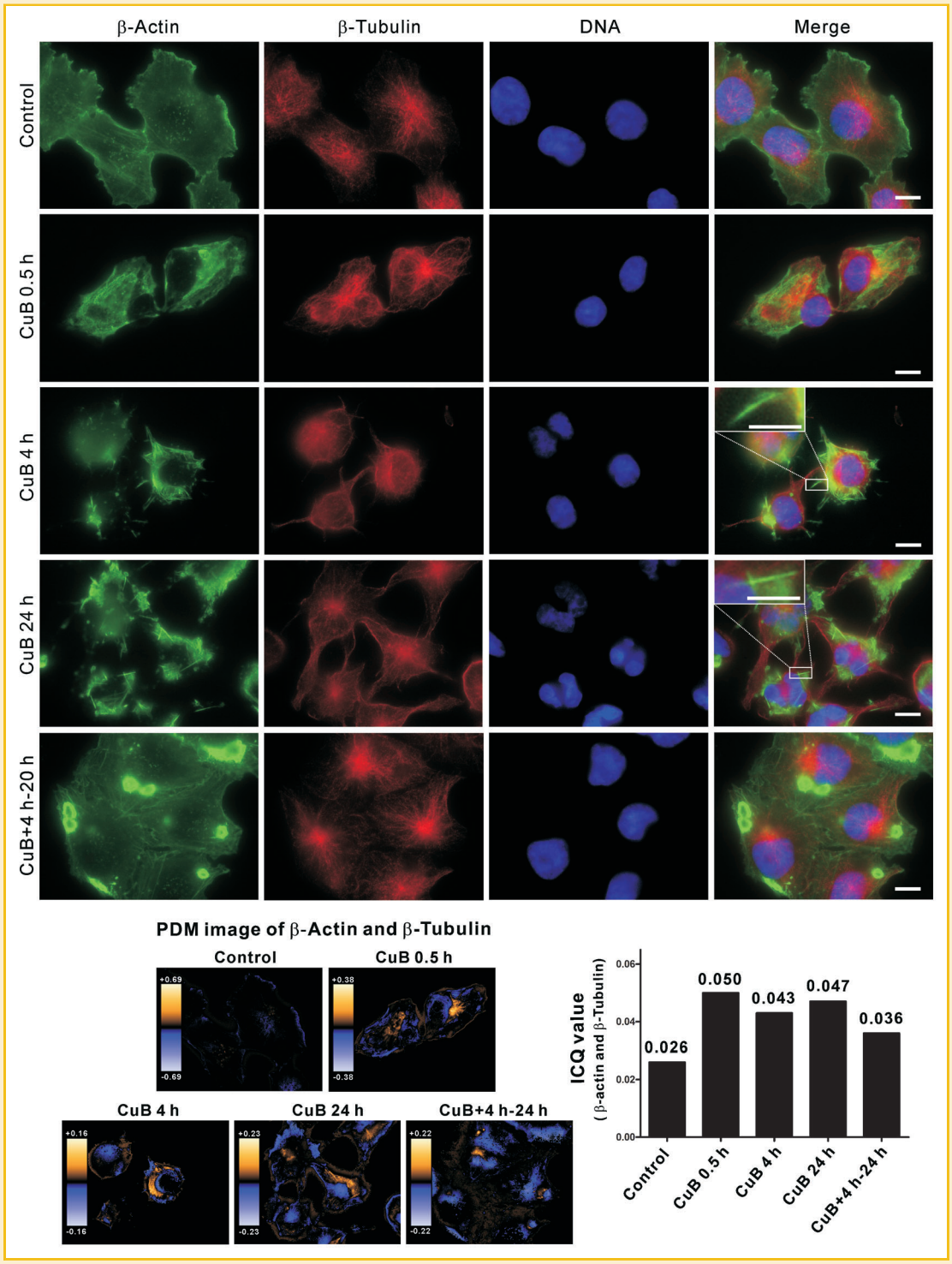

Fig. 1. Immunofluorescence microscopy analysis of actin and tubulin in CuB-treated A375 melanoma cells. A375 cells were treated with CuB (0.1 μM) for indicated times and then immunostained with anti-β-actin (green) and anti-β-tubulin (red) antibodies. Nuclei (blue) were revealed by Hoechst33342 staining. Both separated and merged images are shown. Actin was evenly distributed in control cells. CuB induced actin aggregation and formation of rod-like actin structures (4 and 24 h). When A375 cells were cultured in media without CuB for additional 20 h after pulse-exposed with CuB (4 h), the actin rods disappeared and only clusters of amorphous actin aggregates were retained. Colocalization analysis (lower panels) was performed using Intensity Correlation Analysis (ICA) method. Product of the Differences from the Mean (PDM) images and Intensity Correlation Quotient (ICQ) values (lower right panel) are shown. See Materials and Methods Section for more details. Magnified images of the boxed areas (merged images) are presented in the insets. Scale bars: 10 μm (5 μm in insets).

et al., 2005; Bamburg and Bernstein, 2010]. As cucurbitacin E has been shown to induce cofilin activation [Nakashima et al., 2010], we examined whether cofilin was also activated after CuB treatment. Western blot analysis showed that cofilin was rapidly hyperactivated by CuB in a dose-dependent manner (Fig. 2A and Supplementary Fig. S4A). We then analyzed the subcellular distribution of cofilin and its relation with actin rods in CuB-treated cells. Immunofluorescence microscopy revealed that the cofilin molecules were first clustered into clumps, which were colocalized with the amorphous actin aggregates (Fig. 2B, 0.5 h). Subsequently needle-like actin and cofilin rods were observed (Fig. 2B, 4 h). The cofilin rods were highly colocalized with the actin rods in both A375 cells (Fig. 2B, 4 h) and B16F10 cells (Supplementary Fig. S4B), indicating that they were actually cofilin–actin rods [Minamide et al., 2010]. After exposure to CuB for 24 h, these cofilin–actin rods were still visible (Fig. 2B, 24 h). Together, these results suggested that CuB-induced actin aggregates and cofilin–actin rods correlated with cofilin hyperactivation.

COFILIN HYPERACTIVATION AND COFILIN–ACTIN ROD FORMATION WERE DOWNSTREAM EVENTS OF ACTIN AGGREGATION

Previously, we have demonstrated that NAC pretreatment alleviates CuB-induced G-actin depletion, although the underlying mechanism is unclear [Zhang et al., 2011]. Such an effect of NAC could also be observed in CuB-treated A375 cells (Supplementary Fig. S2B). We thus used this agent as a tool to study the correlation between CuB-induced cofilin activation and actin aggregation. As shown in Figure 3A, NAC (10 mM) alone did not change the subcellular distribution of actin and cofilin, whereas NAC pretreatment not only suppressed CuB-induced actin aggregation but also abolished the formation of cofilin–actin rods in A375 cells. Interestingly, CuB-induced cofilin hyperactivation was markedly suppressed in the presence of NAC while NAC itself had no effect on cofilin activation (Fig. 3B).

To further explore its roles in actin aggregation and cofilin–actin rod formation, cofilin was knocked down by siRNA in A375 cells. As shown in Figure 3C, cofilin levels were reduced by nearly 60% at 72 h post-transfection. Interestingly, when cofilin expression was significantly decreased by siRNA knockdown, hence abolishing the possibility of cofilin hyperactivation, actin aggregation still took place in cofilin-knockdown cells upon exposure to CuB (Fig. 3D). However, actin rod formation was markedly suppressed in cofilin-knockdown cells, whereas cofilin–actin rods were still observed in those cells in which cofilin was not significantly reduced (Fig. 3D), indicating an indispensable role of cofilin in actin rod formation. Taken together, these results demonstrated that CuB-induced actin aggregation did not rely on the expression and hyperactivation of cofilin, but rather resulted in cofilin hyperactivation and cofilin–actin rod formation.

COFILIN HYPERACTIVATION UPON CUCURBITACIN-B TREATMENT WAS SLINGSHOT HOMOLOG 1-DEPENDENT BUT WAS CHRONOPHIN-INDEPENDENT

Slingshot phosphatases (SSH, including SSH1, 2 and 3) and CIN are the major phosphatases responsible for cofilin activation in modulating actin dynamics [Ghosh et al., 2004; Gohla et al., 2005; Huang et al., 2008; Van Troys et al., 2008]. As SSH1 can associate with F-actin and may be the major SSH isoform in regulating cofilin activity [Niwa et al., 2002; Nagata-Ohashi et al., 2004], we examined its role in CuB-induced cofilin hyperactivation and cofilin–actin rod formation. Western blot analysis showed that the expression of SSH1 was significantly increased in A375 cells after 24 h of CuB treatment (Fig. 4A). We then analyzed the subcellular distribution of SSH1 and its correlation with actin aggregation in CuB-treated cells. Immunofluorescence microscopy revealed that SSH1 was significantly colocalized with actin aggregates induced by CuB (Fig. 4B, 4 h). Furthermore, we performed siRNA-mediated knockdown of SSH1 gene in A375 cells. The SSH1 protein levels were reduced by nearly 80% (Fig. 5A) and CuB-induced cofilin activation was greatly alleviated after SSH1 siRNA transfection for 72 h as compared with negative siRNA control (Fig. 5A). Importantly, actin aggregation was induced but cofilin–actin rod formation was suppressed in SSH1-knockdown cells (Fig. 5B). By contrast, in control siRNA transfected cells, CuB could still rapidly induce actin aggregation and cofilin–actin rod formation (data not shown). These results indicated that SSH1 contributed, at least partially, to the cofilin hyperactivation which was required for the cofilin–actin rod formation.

Next, we sought to determine whether CIN had participated in the cofilin activation in CuB-treated cells. Western blot analysis revealed that there were little changes in the expression levels of CIN in the cells treated with CuB for different time lengths (Fig. 6A). Moreover, in the cells that CIN expression was reduced by nearly 75% upon siRNA-mediated knockdown (Fig. 6B), we found that CuB-induced actin aggregation, cofilin hyperactivation, and cofilin–actin rod formation had not been influenced (Fig. 6B,C). By contrast, the formation of actin stress fibers was enhanced in CIN-knockdown cells (Fig. 6C), in line with a previous study showing the involvement of CIN in actin stress fiber reorganization [Gohla et al., 2005]. These results suggested that CIN had not been involved in CuB-induced cofilin hyperactivation and cofilin–actin rod formation in melanoma cells.

MODULATION OF CUCURBITACIN-B-INDUCED COFILIN HYPERACTIVATION BY ROCK/LIMK SIGNALING PATHWAY

Apart from the phosphatases SSH and CIN, the LIMK1/2 and their upstream kinase ROCK1 may also regulate cofilin activation [Lin et al., 2003; Scott and Olson, 2007]. Therefore, we next determined whether the ROCK/LIMK pathway had been involved in CuB-induced cofilin hyperactivation and cofilin–actin rod formation. Western blot analysis showed that the phosphorylated (active) forms of LIMK1/2 were downregulated whereas the expression level of total LIMK2 was not changed (Fig. 7A,C). ROCK1, the upstream kinase of LIMK1/2, was also downregulated (Fig. 7A,D). Thus, ROCK1 downregulation might contribute to the decrease of phosphorylated LIMK1/2. As the downregulation of ROCK/LIMK signaling took place later than the cofilin activation (Fig. 7A,B), it might contribute to CuB-induced cofilin hyperactivation at later time points, maintaining the prolonged cofilin activation.

ANALYSIS OF REACTIVE OXYGEN SPECIES LEVELS IN CUCURBITACIN-B-TREATED CELLS

Previously, we have demonstrated that pretreatment with NAC, a well-known reactive oxygen species (ROS) scavenger that contains a

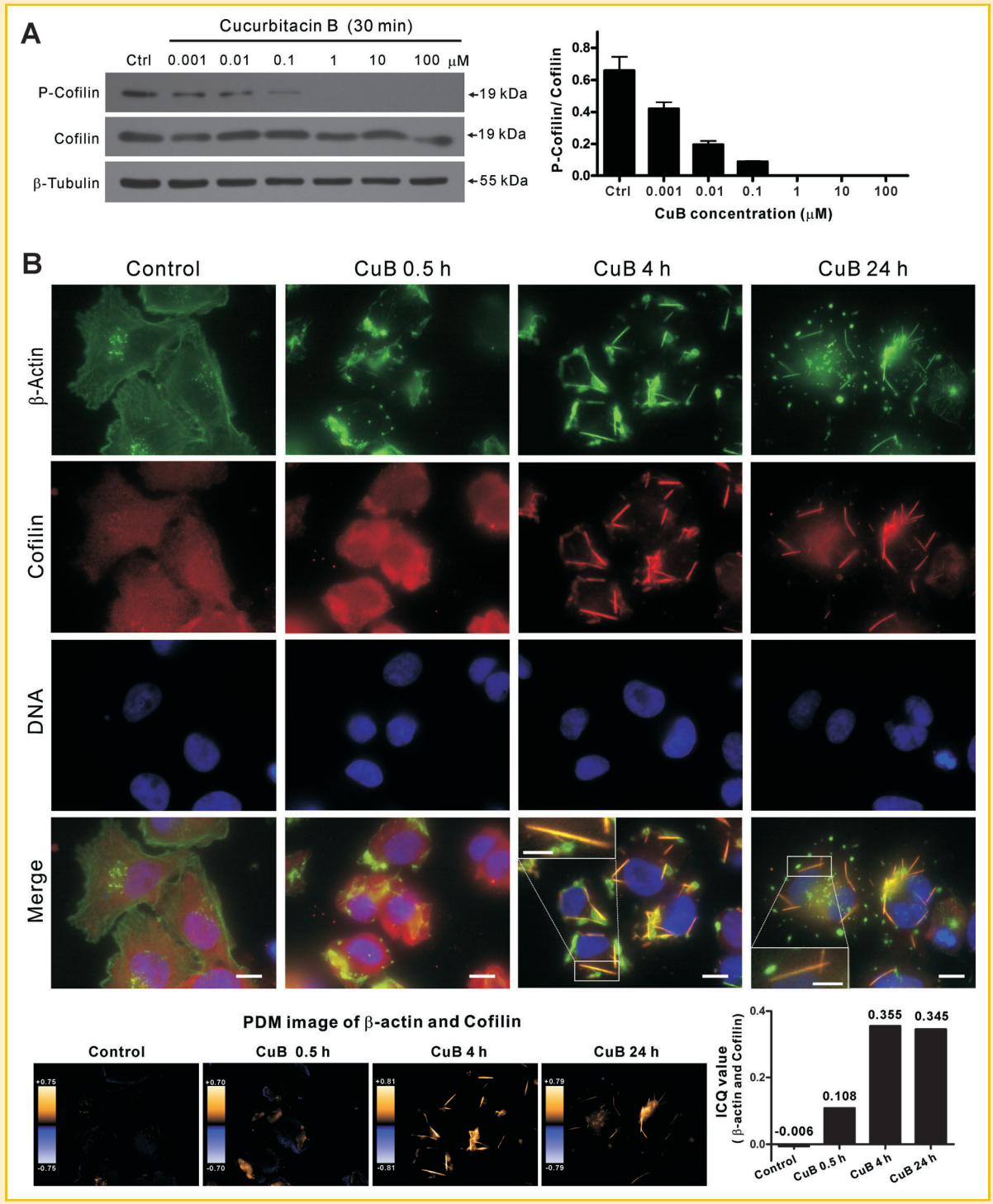

Fig. 2. Cofilin dephosphorylation (activation) and cofilin–actin rod formation in A375 cells. A: CuB treatment dose-dependently induced cofilin dephosphorylation. Cells were treated with CuB (0.001–100 μM) for 30 min. Cell lysates were collected and analyzed by Western blotting. Quantitative assessment of Western blotting is shown on the right. B: Cofilin–actin rods were induced in CuB-treated cells. Cells were treated with CuB (0.1 μM) for indicated times and were immunostained with anti-β-actin (green) and anti-cofilin (red) antibodies. The fluorescent images were visualized by immunofluorescence microscopy. Nuclei (blue) were revealed by Hoechst33342 staining. Both separated and merged images are shown. Magnified images of the boxed areas are presented as insets in merged images. Colocalization analysis (lower panels) was performed using ICA method. Both PDM images and ICQ values (lower right panel) are shown. Cofilin rods were colocalized with actin rods (yellow) in cells treated with CuB. Scale bars: 10 μm (5 μm in insets).

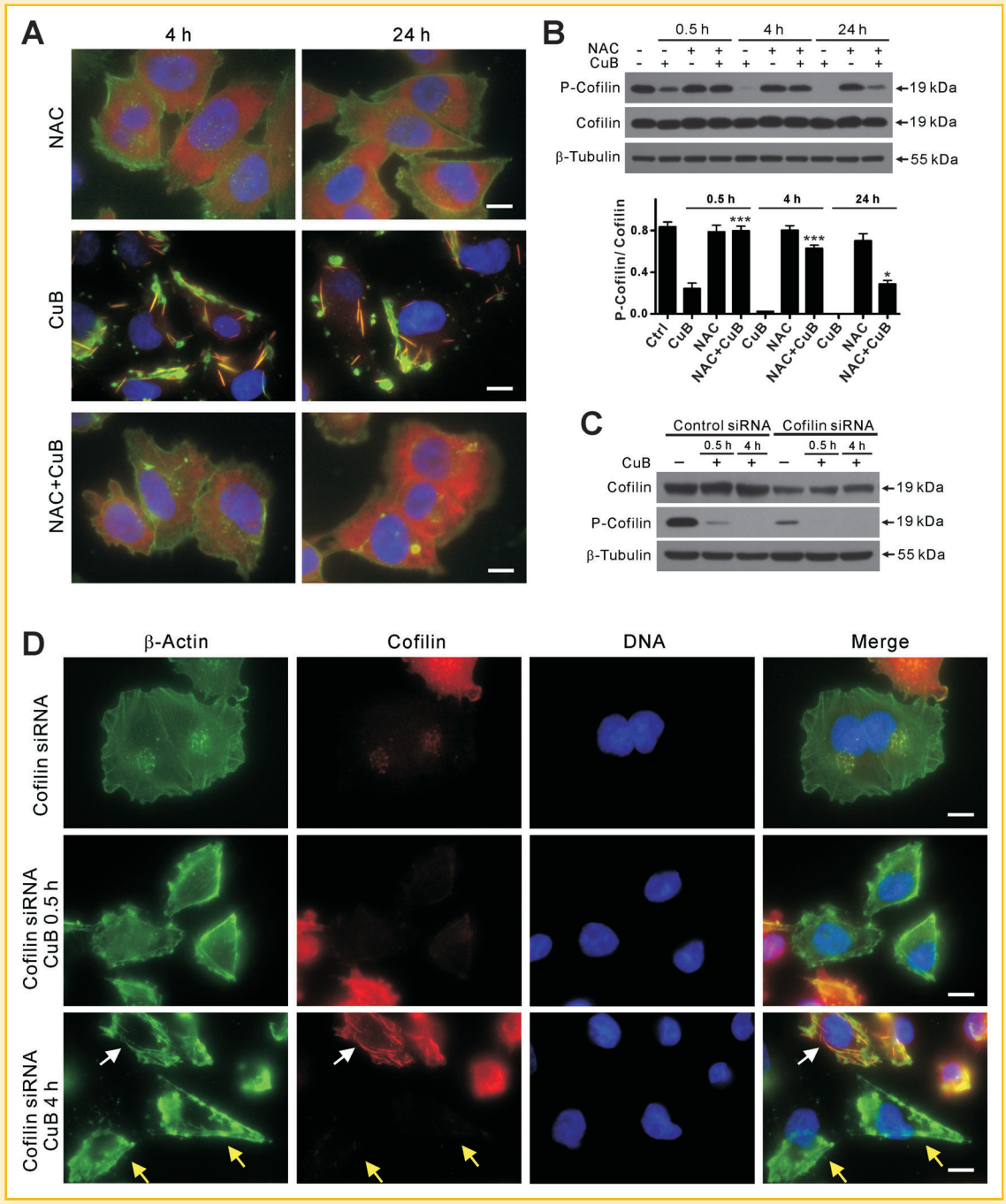

Fig. 3. Influence of NAC pretreatment and cofilin knockdown on CuB-induced cofilin dephosphorylation and cofilin–actin rod formation. A: Immunofluorescence microscopy analysis of the influence of NAC pretreatment on CuB-induced cofilin–actin rod formation in A375 cells. Cells were pretreated with NAC (10 mM) for 1 h before exposure to CuB (0.1 μM) for indicated times. Actin and cofilin were immunostained with anti-β-actin (green) and anti-cofilin (red) antibodies, respectively. Nuclei (blue) were revealed by Hoechst33342 staining. The merged images are shown. Scale bars: 10 μm. B: Effect of NAC pretreatment on CuB-induced cofilin dephosphorylation. Cell lysates were extracted from 0.1 μM CuB-treated or 10 mM NAC-pretreated cells at indicated time points, and protein expression levels were analyzed by Western blotting. β-Tubulin was used as equal loading control. The relative densitometry values as compared to cofilin are presented (right). $^{*}P < 0.05$ and $^{***}P < 0.001$ versus CuB. C: Influence of cofilin knockdown on CuB-induced cofilin dephosphorylation. A375 cells were transfected with negative control (Control) or cofilin siRNA duplexes at a final concentration of 40 nM for 72 h and then treated with CuB (0.1 μM) for indicated times. Cell lysates were collected and analyzed by Western blotting. D: Immunofluorescence microscopy analysis of the influence of cofilin knockdown on actin and cofilin dynamics in A375 cells treated with CuB. After cofilin knockdown (see above) and treated with CuB, A375 cells were immunostained with anti-β-actin (green) and anti-cofilin (red) antibodies. Nuclei (blue) were revealed by Hoechst33342 staining. The white arrows indicate the cell in which cofilin was not efficiently knocked down, while the yellow arrows indicate the cells in which cofilin was significantly knocked down. Scale bars: 10 μm.

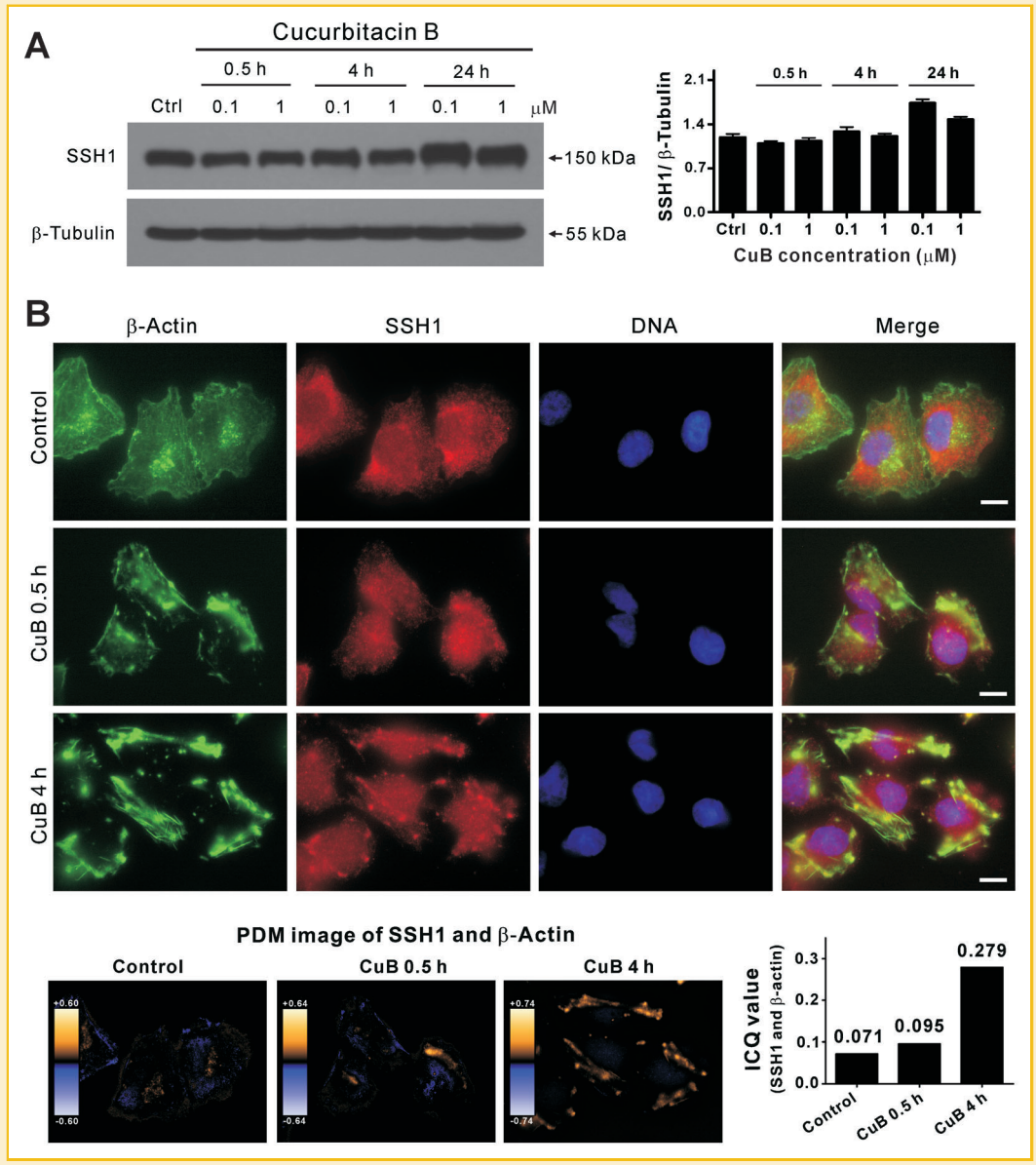

Fig. 4. Regulation of Slingshot homolog 1 (SSH1) in CuB-treated A375 melanoma cells. A: CuB increased the expression of SSH1. Cell lysates were extracted from cells after treatment with graded doses of CuB at indicated time points, and protein expression levels were analyzed by Western blotting. β-Tubulin was used as equal loading control. The relative densitometry values compared to β-tubulin are presented. B: Immunofluorescence microscopy analysis of SSH1 and actin in CuB-treated melanoma cells. A375 cells were treated with CuB (0.1 μM) for indicated times and then immunostained with anti-β-actin (green) and anti-SSH1 (red) antibodies. Nuclei (blue) were revealed by Hoechst33342 staining. Both separated and merged images are shown. Colocalization analysis (lower panels) was performed using ICA method, PDM images and ICQ values (lower right panel) are shown. SSH1 was co-existed with actin aggregates (yellow) in cells treated with CuB. Scale bars: 10 μm.

thiol group, significantly alleviated CuB-induced actin aggregation [Zhang et al., 2011]. We thus sought to explore whether ROS had been involved in the action of CuB. To resolve this issue, we detected ROS levels with or without CuB treatment by pre-loading cells with H_2DCF-DA and found that CuB treatment did not elevate, but rather slightly reduced the cellular ROS level (Supplementary Fig. S5), consistent with our previous study in B16F10 cells [Zhang et al., 2011]. Pretreatment of the cells with NAC or other ROS inhibitors, including DPI and VAS2870 (VAS) that contain no thiol groups, reduced the basal ROS level in control cells and the ROS level in CuB-treated cells (Fig. 8A). Furthermore, NAC pretreatment not only alleviated CuB-induced cell membrane shrinking (Fig. 8B) and cofilin activation (Figs. 3B and 8C), but also reduced CuB-induced actin aggregation and cofilin–actin rod formation (Fig. 3A). However, such effects were not observed when the cells were pretreated with DPI and VAS (Fig. 8C,D). These results suggested that ROS was not directly involved in CuB-induced actin aggregation whereas thiol oxidation might have a role in this process.

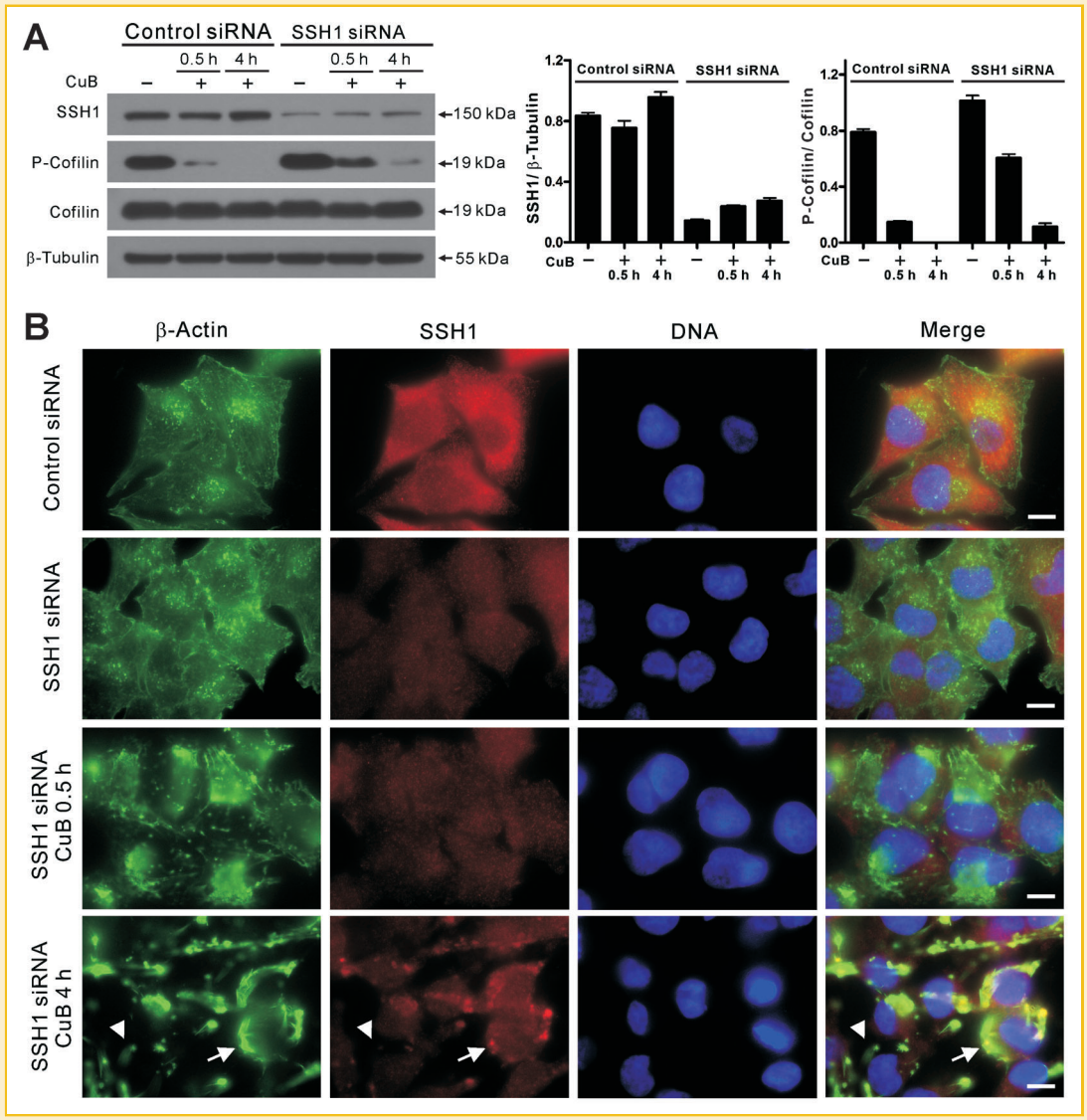

Fig. 5. Effect of SSH1 knockdown on CuB-induced cofilin dephosphorylation and actin aggregation in A375 cells. A: Knockdown of SSH1 alleviated CuB-induced cofilin dephosphorylation. A375 cells were transfected with negative control (Control) or SSH1 siRNA at a final concentration of 20 nM for 72 h and then treated with CuB (0.1 μM) for indicated times. Cell lysates were collected and subjected to Western blot analysis. Quantitative assessment of Western blotting is shown on the right. B: Immunofluorescence microscopy analysis of the influence of SSH1 knockdown on CuB-induced actin aggregation. Cells were immunostained with anti-β-actin (green) and anti-SSH1 (red) antibodies. Nuclei (blue) were revealed by Hoechst33342 staining. Both separated and merged images are shown. The white arrows indicate the cells in which SSH1 was not efficiently knocked down. The white arrowheads indicate the cell in which SSH1 was significantly knocked down. Scale bars: 10 μm.

DISCUSSION

Cucurbitacins have long been noticed to disrupt actin cytoskeleton in tumor cells [Duncan et al., 1996]. We observed that CuB treatment initially disrupted the actin dynamics leading to actin aggregation and subsequently exhibited the inhibitory effects on cell growth and migration in melanoma cells. Interestingly, we found that cofilin–actin rods were generated following CuB-induced actin aggregation. Cofilin was persistently hyperactivated in CuB-treated cells. By knockdown of cofilin's upstream phosphatases SSH1 and CIN with siRNA, we demonstrated that SSH1, instead of CIN, at least partially contributed to the hyperactivation of cofilin. Notably, the cofilin hyperactivation and cofilin–actin rod formation were downstream events of CuB-induced actin aggregation since cofilin knockdown blocked rod formation but did not affect actin aggregation.

Our finding that cofilin was hyperactivated by CuB treatment is in agreement with a previous report conducted in U937 cells [Nakashima et al., 2010]. However, it has not previously been determined how cofilin was activated in cucurbitacin-treated cells to our best knowledge. As a critical regulator for actin dynamics, cofilin is strictly regulated by several upstream pathways involving SSH, CIN, and ROCK/LIMKs [Meberg et al., 1998; Niwa et al., 2002; Wang et al., 2007]. On the one hand, cofilin activation is achieved via dephosphorylation mediated by SSH, CIN and other phosphatases [Niwa et al., 2002; Huang et al., 2006]. Our data supports the role of SSH1, but not CIN, in CuB-induced cofilin hyperactivation. However,

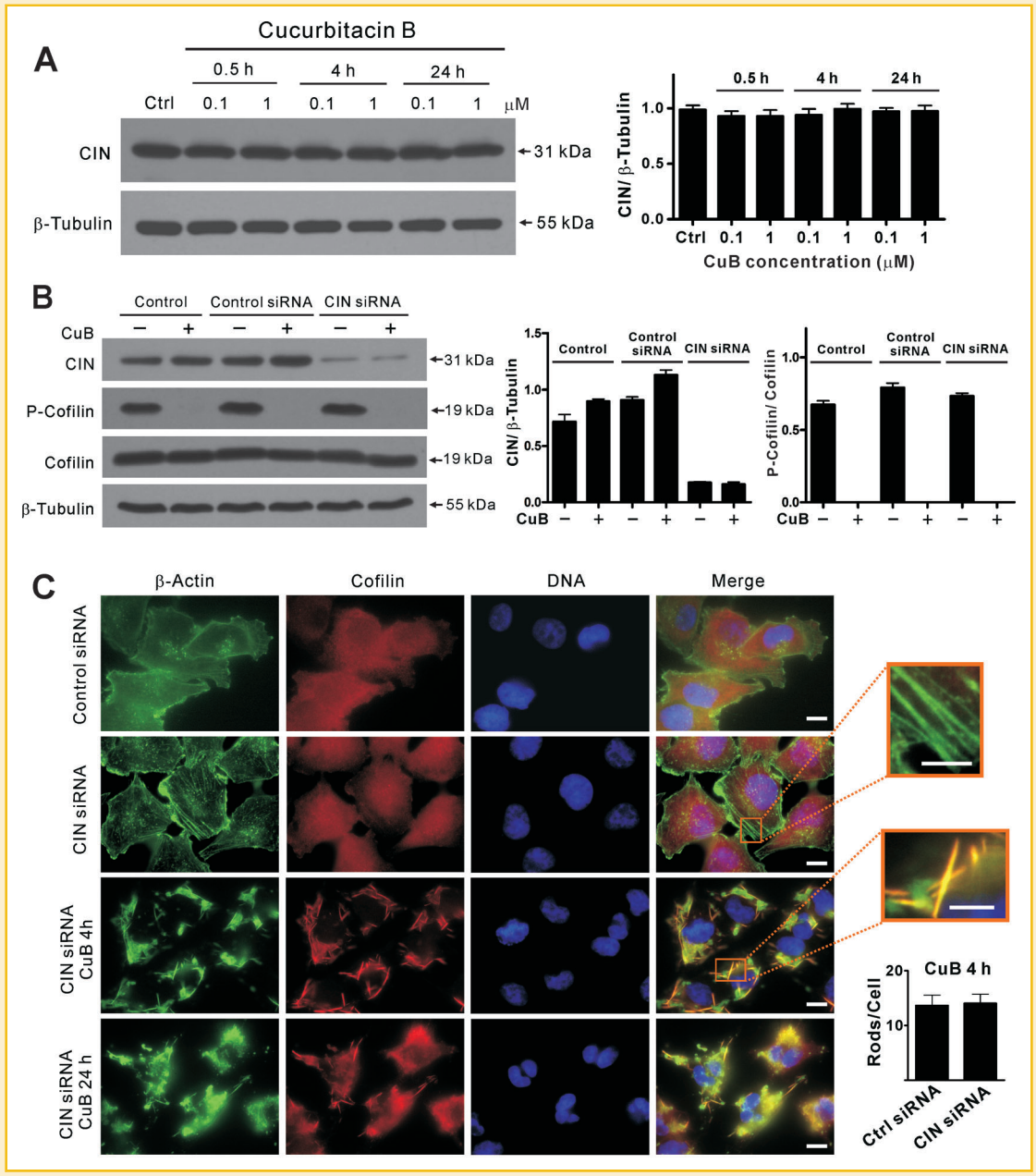

Fig. 6. Analysis of CIN involvement in CuB-induced cofilin dephosphorylation and actin aggregation in A375 cells. A: The expression of CIN was not affected after CuB treatment. Cell lysates were extracted from cells after treatment with graded doses of CuB at indicated time points, and protein expression levels were analyzed by Western blotting. β-Tubulin was used as equal loading control. The relative densitometry values compared to β-tubulin are presented. B: Knockdown of CIN did not affect CuB-induced cofilin dephosphorylation. A375 cells were transfected with negative control (Control) or CIN siRNA at a final concentration of 20 nM for 72 h and then treated with CuB (0.1 μM) for 4 h. Cell lysates were collected and subjected to Western blot analysis. Quantitative assessment of Western blotting is shown on the right. Magnified images of the boxed areas are presented as insets in merged images. C: Immunofluorescence microscopy analysis of the influence of CIN knockdown on CuB-induced actin aggregation. Cells were immunostained with anti-β-actin (green) and anti-cofilin (red) antibodies. Nuclei (blue) were revealed by Hoechst33342 staining. The merged images and the enlarged fibers and rods are shown. Quantitative assessment of rods from 10 cells is shown. Scale bar: 10 μm (5 μm in insets).

we cannot exclude the involvement of other SSH isoforms as well as other phosphatases [Niwa et al., 2002; Huang et al., 2006], which may account for why cofilin phosphorylation could only partially be restored after SSH1 knockdown. On the other hand, as cofilin phosphorylation can be regulated by ROCK/LIMK signaling [Lin et al., 2003; Scott and Olson, 2007], downregulation of LIMK activity may decrease the level of cofilin phosphorylation [Van Troys et al., 2008]. In line with these reports, we found that the phosphorylation levels of LIMK1/2 as well as the expression levels of ROCK1 were significantly decreased after CuB treatment for 4 h. However, the downregulation of ROCK/LIMK signaling took place after the activation of cofilin since the latter started at as early as

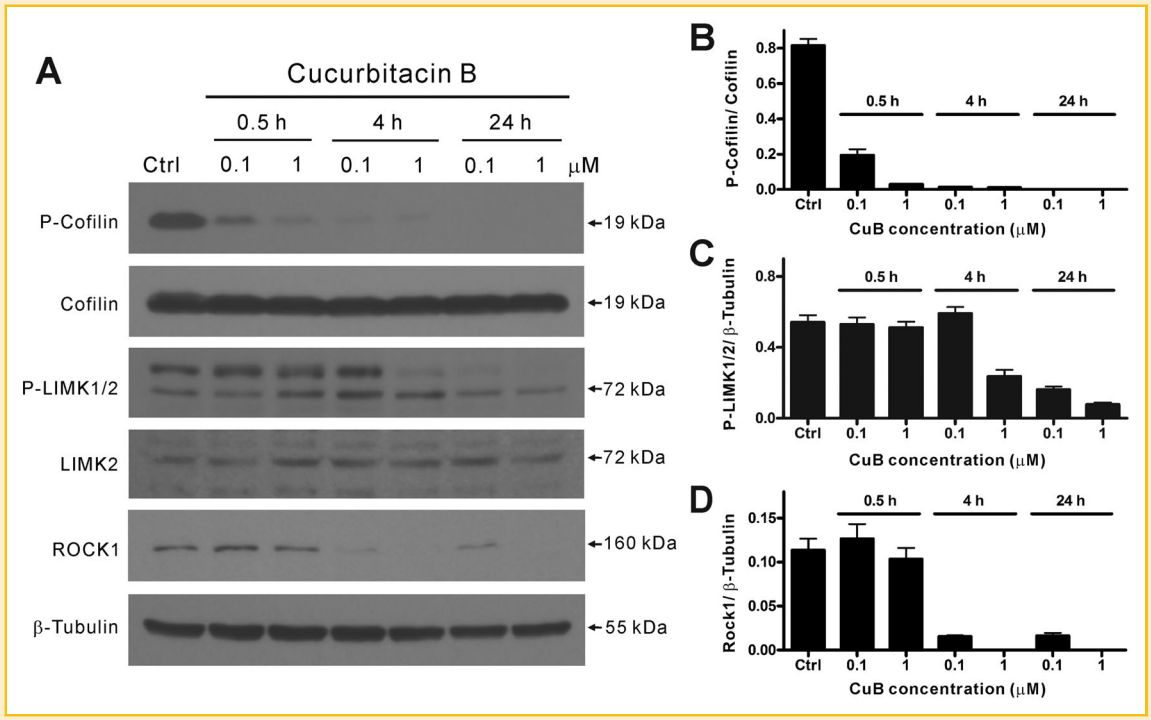

Fig. 7. Modulation of ROCK/LIMK signaling in A375 cells treated with CuB. Cell lysates were extracted from cells after treatment with graded doses of CuB at indicated time points, and protein expression levels were analyzed by Western blotting using specific antibodies (A). β-Tubulin was used as equal loading control. The relative densitometry values compared to cofilin or β-tubulin are presented for each protein (B–D). ROCK/LIMK signaling was downregulated after exposure to CuB for 4 h.

0.5 h. Therefore, ROCK/LIMK signaling might not be the trigger of cofilin activation but might contribute to the maintenance of prolonged cofilin activation by CuB.

Apart from cofilin hyperactivation, we observed a robust formation of cofilin–actin rods in CuB-treated cells. As far as we know, these cofilin–actin rods have not been reported in previous studies on cucurbitacins [Duncan et al., 1996; Yin et al., 2008; Knecht et al., 2010; Boykin et al., 2011]. One explanation is that we used anti-β-actin and anti-cofilin antibodies to illuminate the rod structure whereas the previous studies adopted fluorescent phalloidin, which cannot bind to the actin filaments embedded in cofilin rods [Nishida et al., 1987; Bamburg, 1999]. It is well-known that the activated cofilin can bind to and sever F-actin filaments. However, when cofilin-to-actin ratio reaches a critical level (i.e., 1:1), the active cofilin will initiate the formation of rod-shaped and cofilin-saturated actin filament bundles (i.e., cofilin–actin rods), rather than severing F-actin [Nishida et al., 1987; Andrianantoandro and Pollard, 2006; Van Troys et al., 2008]. Previous studies have demonstrated that a variety of treatments, including cofilin overexpression, ATP depletion, oxidative stress, glutamate-induced excitotoxicity, and small soluble forms of amyloid-β peptide (Aβ-(1–42)), induce cofilin–actin rod formation in cultured neurons and these rods vary from needle- to sausage-shaped inclusions [Jang et al., 2005; Maloney et al., 2005; Huang et al., 2008; Minamide et al., 2010; Bernstein et al., 2012]. In addition to neurons, different types of cells have been demonstrated to form cofilin–actin rods in response to declined cellular ATP or 10% DMSO treatment [Nishida et al., 1987; Ono et al., 1996]. More importantly, these treatments that cause cofilin–actin rod formation also induce cofilin dephosphorylation (activation) [Minamide et al., 2000; Jang et al., 2005; Maloney et al., 2005; Huang et al., 2008], indicating a key role of activated cofilin in intracellular rod formation. In line with these studies, our data also revealed a robust activation of cofilin followed by cofilin–actin rod formation after CuB treatment and this cofilin hyperactivation was maintained persistently. Furthermore, the suppression of cofilin activity by siRNA knockdown or by NAC treatment correlated with the blockade of rod formation. Thus, cofilin hyperactivation was essential for the reorganization of CuB-induced actin aggregates into cofilin–actin rods.

Although cofilin knockdown blocked the formation of actin rods, it had little effect on the formation of CuB-induced actin aggregates. Moreover, knockdown of SSH1 expression significantly mitigated CuB-induced cofilin hyperactivation and cofilin–actin rod formation, but did not suppress the formation of amorphous actin aggregates. Previous studies have indicated that binding of the C-terminal domain of SSH1 to F-actin is a prerequisite for the activation of the phosphatase as the C-terminal domain is auto-inhibitory to its activity [Nagata-Ohashi et al., 2004; Soosairajah et al., 2005; Huang et al., 2006]. We thus hypothesized that the CuB-induced actin aggregates recruited and thus activated SSH1, leading to the cofilin activation. In line with this hypothesis, CuB-induced actin aggregates was observed to be colocalized with SSH1. In contrast to SSH1, knockdown of CIN expression neither reduced CuB-induced actin aggregation nor suppressed cofilin hyperactivation and cofilin–actin

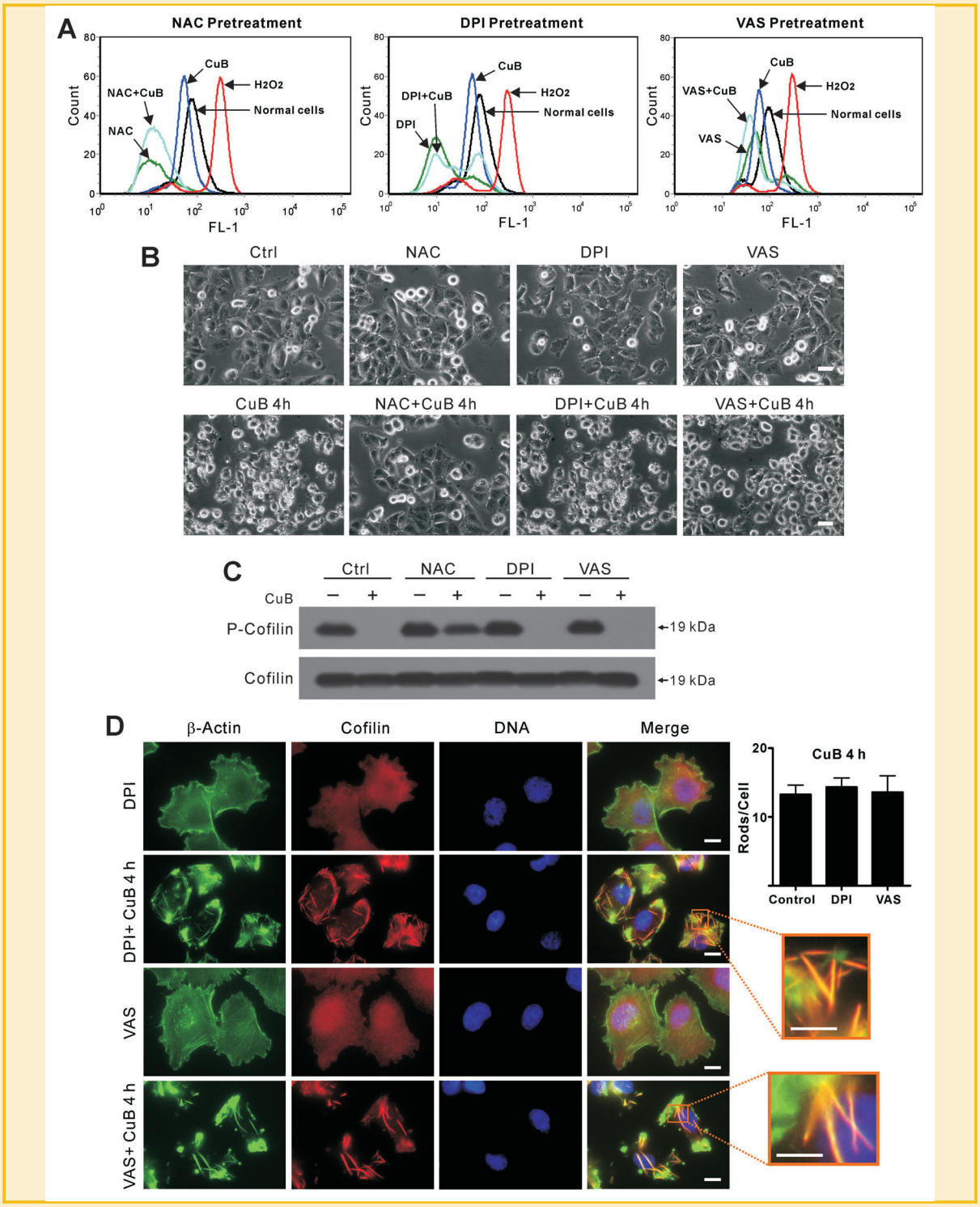

Fig. 8. Effects of ROS inhibitors on CuB-induced cofilin dephosphorylation and cofilin–actin rod formation in A375 cells. A: Effect of ROS inhibitors NAC, DPI (diphenyleneiodonium chloride) or VAS (VAS2870) pretreatment on ROS levels in A375 cells. Cells were treated with CuB (0.1 μM) alone for 30 min or pretreated with NAC (10 mM), DPI (10 μM), or VAS (20 μM) for 1 h followed by CuB (0.1 μM) treatment for 30 min. ROS level in cells was analyzed using flow cytometry. B–D: Comparison of the influence of NAC, DPI, or VAS pretreatment on CuB-induced cell morphological changes (B), cofilin dephosphorylation (C), and cofilin–actin rod formation (D). A375 cells were treated with CuB (0.1 μM) alone for 4 h or pretreated with NAC (10 mM), DPI (10 μM), or VAS (20 μM) for 1 h followed by CuB (0.1 μM) treatment for 4 h. Cell morphology was observed using phase-contrast microscopy (B). Scale bars: 20 μm. Phosphorylated-cofilin and cofilin levels were analyzed using Western blotting (C). (D) In immunofluorescence microscopy analysis, cells were immunostained with anti-β-actin (green) and anti-cofilin (red) antibodies, and nuclei (blue) were revealed by Hoechst33342 staining. Quantitative assessment of rods from10 cells and the enlarged rods are shown on the right. Magnified images of the boxed areas are presented as insets in merged images. Scale bars: 10 μm (5 μm in insets).

rod formation. Therefore, it appeared that CuB-induced actin aggregation resulted in the cofilin hyperactivation which partly depended on SSH1 but not CIN.

However, it is still unknown how the actin aggregation was induced by CuB. Given that actin filaments contain a large amount of free thiol groups and cross-linking of these groups by ROS leads to actin aggregation [DalleDonne et al., 1995; Lum and Roebuck, 2001], we found that NAC, an ROS scavenger, significantly alleviated CuB-induced actin aggregation and cofilin hyperactivation, and completely blocked the cofilin–actin rod formation (Fig. 3 and [Zhang et al., 2011]). However, is intracellular ROS elevated in CuB-treated melanoma cells? To address this issue, we detected the ROS levels with or without CuB treatment and found that CuB did not elevate, but rather reduced cellular ROS level in A375 cells, consistent with our previous study in B16F10 cells [Zhang et al., 2011]. However, our results demonstrated that NAC did reduce the basal ROS level in control cells and further reduced the ROS level in CuB-treated cells (Fig. 8A), in line with its function to scavenge ROS in cells [Att et al., 2009; Hsin et al., 2010]. Similar effects were observed in the cells pretreated with other ROS inhibitors DPI and VAS2870 [Singh et al., 2005; Sun et al., 2012], although their ROS blocking effects were slightly weaker than that of NAC. Unlike NAC, DPI, or VAS2870 did not alleviate the disruption of actin cytoskeleton (cell membrane shrinking) and actin aggregation, nor did they prevent cofilin hyperactivation and cofilin–actin rod formation by CuB treatment (Fig. 8B–D), suggesting that these effects of CuB were not directly mediated by an increase in ROS levels. Thus, other properties of NAC may be responsible for its action on CuB-induced actin aggregation. It is of note that NAC is a thiol-containing reducing reagent, distinguished from DPI and VAS2870, which have no thiol groups. Previous studies have indicated that 14-3-3 proteins are critical regulators of SSH activity. Thiol oxidation of 14-3-3ζ leads to the release of SSH from an inhibitory complex and the activation of the latter [Kim et al., 2009]. The dependence of cofilin recruitment into rods on DTT-sensitive Cys–Cys intermolecular bonds [Bernstein et al., 2012] also suggests that thiol oxidation might have mediated the action of CuB in our study. Therefore, we presumed that CuB might act on some thiol redox proteins that mediated thiol cross-linking between actin molecules and NAC treatment alleviated the actin aggregation by preventing such cross-linking. Yet further investigation is required to clarify this issue.

In conclusion, we demonstrated that cofilin hyperactivation and cofilin–actin rod formation were downstream events of CuB-induced actin aggregation, which was modulated by ROCK/LIMK signaling and SSH but was independent of CIN. Further work is warranted to reveal the direct target(s) of CuB, which may ultimately explain how actin aggregates are formed. Due to its critical role in cell cycle progression and motility [Hall, 2009], CuB-induced disruption of actin cytoskeleton may lead to tumor cell growth arrest and migration inhibition. Moreover, cofilin–actin rod formation plays a critical role in the pathogenesis of neurodegenerative diseases including Alzheimer's disease [Bamburg et al., 2010]. Therefore, a better understanding of the cofilin–actin rods induced by CuB will benefit the application of CuB as an anticancer drug and as a tool for studying cofilin–actin rod dynamics in neurodegenerative diseases.

ACKNOWLEDGMENTS

The authors thank Dr. Barbara W. Bernstein (Colorado State University) for helpful discussion. This work was supported by grants from the National Natural Science Foundation of China (No. 81173604), the Specialized Research Program of "Twelfth Five-Year Plan" of China (2011ZX09307-303-03), and the Fundamental Research Funds for the Central Universities (21611387).

REFERENCES

Andrianantoandro E, Pollard TD. 2006. Mechanism of actin filament turnover by severing and nucleation at different concentrations of ADF/cofilin. Mol Cell 24:13–23.

Att W, Yamada M, Kojima N, Ogawa T. 2009. N-acetyl cysteine prevents suppression of oral fibroblast function on poly(methylmethacrylate) resin. Acta Biomater 5:391–398.

Bamburg JR. 1999. Proteins of the ADF/cofilin family: Essential regulators of actin dynamics. Annu Rev Cell Dev Biol 15:185–230.

Bamburg JR, Bernstein BW. 2010. Roles of ADF/cofilin in actin polymerization and beyond. F1000 Biol Rep 2:62.

Bamburg JR, Bernstein BW, Davis RC, Flynn KC, Goldsbury C, Jensen JR, Maloney MT, Marsden IT, Minamide LS, Pak CW, Shaw AE, Whiteman I, Wiggan O. 2010. ADF/cofilin–actin rods in neurodegenerative diseases. Curr Alzheimer Res 7:241–250.

Bernstein BW, Shaw AE, Minamide LS, Pak CW, Bamburg JR. 2012. Incorporation of cofilin into rods depends on disulfide intermolecular bonds: Implications for actin regulation and neurodegenerative disease. J Neurosci 32:6670–6681.

Boykin C, Zhang G, Chen YH, Zhang RW, Fan XE, Yang WM, Lu Q. 2011. Cucurbitacin IIa: A novel class of anti-cancer drug inducing non-reversible actin aggregation and inhibiting survivin independent of JAK2/STAT3 phosphorylation. Br J Cancer 104:781–789.

Chen JC, Chiu MH, Nie RL, Cordell GA, Qiu SX. 2005. Cucurbitacins and cucurbitane glycosides: Structures and biological activities. Nat Prod Rep 22:386–399.

Chen X, Bao J, Guo J, Ding Q, Lu J, Huang M, Wang Y. 2012. Biological activities and potential molecular targets of cucurbitacins: A focus on cancer. Anticancer Drugs 23:777–787.

DalleDonne I, Milzani A, Colombo R. 1995. H_2O_2-treated actin: Assembly and polymer interactions with cross-linking proteins. Biophys J 69:2710–2719.

DesMarais V, Ghosh M, Eddy R, Condeelis J. 2005. Cofilin takes the lead. J Cell Sci 118:19–26.

Duncan KL, Duncan MD, Alley MC, Sausville EA. 1996. Cucurbitacin E-induced disruption of the actin and vimentin cytoskeleton in prostate carcinoma cells. Biochem Pharmacol 52:1553–1560.

Ghosh M, Song X, Mouneimne G, Sidani M, Lawrence DS, Condeelis JS. 2004. Cofilin promotes actin polymerization and defines the direction of cell motility. Science 304:743–746.

Gohla A, Birkenfeld J, Bokoch GM. 2005. Chronophin, a novel HAD-type serine protein phosphatase, regulates cofilin-dependent actin dynamics. Nat Cell Biol 7:21–29.

Hall A. 2009. The cytoskeleton and cancer. Cancer Metastasis Rev 28:5–14.

Haritunians T, Gueller S, Zhang L, Badr R, Yin D, Xing H, Fung MC, Koeffler HP. 2008. Cucurbitacin B induces differentiation, cell cycle arrest, and actin cytoskeletal alterations in myeloid leukemia cells. Leuk Res 32:1366–1373.

Hsin IL, Sheu G-T, Chen H-H, Chiu L-Y, Wang H-D, Chan H-W, Hsu C-P, Ko J-L. 2010. N-acetyl cysteine mitigates curcumin-mediated telomerase inhibition through rescuing of Sp1 reduction in A549 cells. Mutat Res 688:72–77.

Huang TY, DerMardirossian C, Bokoch GM. 2006. Cofilin phosphatases and regulation of actin dynamics. Curr Opin Cell Biol 18:26–31.

Huang TY, Minamide LS, Bamburg JR, Bokoch GM. 2008. Chronophin mediates an ATP-sensing mechanism for cofilin dephosphorylation and neuronal cofilin–actin rod formation. Dev Cell 15:691–703.

Jang DH, Han JH, Lee SH, Lee YS, Park H, Lee SH, Kim H, Kaang BK. 2005. Cofilin expression induces cofilin–actin rod formation and disrupts synaptic structure and function in aplysia synapses. Proc Natl Acad Sci USA 102:16072–16077.

Jayaprakasam B, Seeram NP, Nair MG. 2003. Anticancer and antiinflammatory activities of cucurbitacins from *Cucurbita andreana*. Cancer Lett 189:11–16.

Kim JS, Huang TY, Bokoch GM. 2009. Reactive oxygen species regulate a slingshot-cofilin activation pathway. Mol Biol Cell 20:2650–2660.

Knecht DA, LaFleur RA, Kahsai AW, Argueta CE, Beshir AB, Fenteany G. 2010. Cucurbitacin I inhibits cell motility by indirectly interfering with actin dynamics. PLoS ONE 5:e14039.

Li Q, Lau A, Morris TJ, Guo L, Fordyce CB, Stanley EF. 2004. A syntaxin 1, Galpha(o), and N-type calcium channel complex at a presynaptic nerve terminal: Analysis by quantitative immunocolocalization. J Neurosci 24:4070–4081.

Lin T, Zeng L, Liu Y, DeFea K, Schwartz MA, Chien S, Shyy JY. 2003. Rho-ROCK-LIMK-cofilin pathway regulates shear stress activation of sterol regulatory element binding proteins. Circ Res 92:1296–1304.

Lum H, Roebuck KA. 2001. Oxidant stress and endothelial cell dysfunction. Am J Physiol Cell Physiol 280:C719–C741.

Maloney MT, Minamide LS, Kinley AW, Boyle JA, Bamburg JR. 2005. Beta-secretase-cleaved amyloid precursor protein accumulates at actin inclusions induced in neurons by stress or amyloid beta: A feedforward mechanism for Alzheimer's disease. J Neurosci 25:11313–11321.

Meberg PJ, Ono S, Minamide LS, Takahashi M, Bamburg JR. 1998. Actin depolymerizing factor and cofilin phosphorylation dynamics: Response to signals that regulate neurite extension. Cell Motil Cytoskeleton 39:172–190.

Minamide LS, Striegl AM, Boyle JA, Meberg PJ, Bamburg JR. 2000. Neurodegenerative stimuli induce persistent ADF/cofilin–actin rods that disrupt distal neurite function. Nat Cell Biol 2:628–636.

Minamide LS, Maiti S, Boyle JA, Davis RC, Coppinger JA, Bao Y, Huang TY, Yates J, Bokoch GM, Bamburg JR. 2010. Isolation and characterization of cytoplasmic cofilin–actin rods. J Biol Chem 285:5450–5460.

Momma K, Masuzawa Y, Nakai N, Chujo M, Murakami A, Kioka N, Kiyama Y, Akita T, Nagao M. 2008. Direct interaction of cucurbitacin E isolated from *Alsomitra macrocarpa* to actin filament. Cytotechnology 56:33–39.

Nagata-Ohashi K, Ohta Y, Goto K, Chiba S, Mori R, Nishita M, Ohashi K, Kousaka K, Iwamatsu A, Niwa R, Uemura T, Mizuno K. 2004. A pathway of neuregulin-induced activation of cofilin-phosphatase slingshot and cofilin in lamellipodia. J Cell Biol 165:465–471.

Nakashima S, Matsuda H, Kurume A, Oda Y, Nakamura S, Yamashita M, Yoshikawa M. 2010. Cucurbitacin E as a new inhibitor of cofilin phosphorylation in human leukemia U937 cells. Bioorg Med Chem Lett 20:2994–2997.

Nishida E, Iida K, Yonezawa N, Koyasu S, Yahara I, Sakai H. 1987. Cofilin is a component of intranuclear and cytoplasmic actin rods induced in cultured cells. Proc Natl Acad Sci USA 84:5262–5266.

Niwa R, Nagata-Ohashi K, Takeichi M, Mizuno K, Uemura T. 2002. Control of actin reorganization by slingshot, a family of phosphatases that dephosphorylate ADF/cofilin. Cell 108:233–246.

Ono S, Abe H, Obinata T. 1996. Stimulus-dependent disorganization of actin filaments induced by overexpression of cofilin in C2 myoblasts. Cell Struct Funct 21:491–499.

Scott RW, Olson MF. 2007. LIM kinases: Function, regulation and association with human disease. J Mol Med (Berl) 85:555–568.

Singh SV, Srivastava SK, Choi S, Lew KL, Antosiewicz J, Xiao D, Zeng Y, Watkins SC, Johnson CS, Trump DL, Lee YJ, Xiao H, Herman-Antosiewicz A. 2005. Sulforaphane-induced cell death in human prostate cancer cells is initiated by reactive oxygen species. J Biol Chem 280:19911–19924.

Soosairajah J, Maiti S, Wiggan O, Sarmiere P, Moussi N, Sarcevic B, Sampath R, Bamburg JR, Bernard O. 2005. Interplay between components of a novel LIM kinase-slingshot phosphatase complex regulates cofilin. EMBO J 24:473–486.

Sun QA, Hess DT, Wang B, Miyagi M, Stamler JS. 2012. Off-target thiol alkylation by the NADPH oxidase inhibitor 3-benzyl-7-(2-benzoxazolyl)thio-1,2,3-triazolo[4,5-d]pyrimidine (VAS2870). Free Radic Biol Med 52:1897–1902.

Van Troys M, Huyck L, Leyman S, Dhaese S, Vandekerkhove J, Ampe C. 2008. Ins and outs of ADF/cofilin activity and regulation. Eur J Cell Biol 87:649–667.

Wang W, Eddy R, Condeelis J. 2007. The cofilin pathway in breast cancer invasion and metastasis. Nat Rev Cancer 7:429–440.

Yin D, Wakimoto N, Xing H, Lu D, Huynh T, Wang X, Black KL, Koeffler HP. 2008. Cucurbitacin B markedly inhibits growth and rapidly affects the cytoskeleton in glioblastoma multiforme. Int J Cancer 123:1364–1375.

Zdanov S, Klamt F, Shacter E. 2010. Importance of cofilin oxidation for oxidant-induced apoptosis. Cell Cycle 9:1675–1677.

Zhang Y, Ouyang D, Xu L, Ji Y, Zha Q, Cai J, He X. 2011. Cucurbitacin B induces rapid depletion of the G-actin pool through reactive oxygen species-dependent actin aggregation in melanoma cells. Acta Biochim Biophys Sin (Shanghai) 43:556–567.

SUPPORTING INFORMATION

Additional supporting information may be found in the online version of this article at the publisher's web-site.

Fig. S1. Inhibitory effect of CuB on human melanoma A375 cells. A: MTS assays measuring the effect of CuB on proliferation of A375 cells. Cells (4×10^3 cells/well) were seeded in 96-well plates for 24 h and then treated with graded doses of CuB (0.01–100 μM) or vehicle (0.1% DMSO) for 24 or 48 h. Data are presented as mean ± SD. $^{**}P < 0.01$ versus CuB. B: Comparison of the proliferation inhibitory effect of CuB on A375 cells in the presence and absence of *N*-acetyl cysteine (NAC). In NAC plus CuB groups, cells were pretreated with NAC (10 mM) 1 h before exposure to CuB (0.01 and 0.1 M). The cells were further cultured for 48 h and measured using MTS assays. C: Effect of CuB on cell cycle distribution of A375 cells. Cells were incubated with CuB (0.1 μM) for 24 or 48 h, and their cell cycle distribution was analyzed by flow cytometry. The percentages of the indicated phases of the cells are presented within each plot (A: apoptosis; T: tetraploid). D: Effect of CuB (0.1 μM) on the migration ability of A375 cells. Cell migration was measured by wound-healing assay with or without pretreatment of NAC (10 mM). Wound width in terms of pixels was quantified (right). Data are presented as mean ± SD. $^{**}P < 0.01$ versus 0 h.

Fig. S2. Analysis of G-actin pool levels in CuB-treated A375 cells. A: G-actin pool was rapidly depleted by CuB in A375 melanoma cells. Cells were treated with CuB (0.1 or 1 μM) or vehicle (0.1% DMSO) for indicated times. G-actin was extracted with 0.2% Triton X-100 and the residues were lysed using two loading buffer for SDS–PAGE. For each lane, 10 μg of total proteins extracted from treated cells were stained with Coomassie Brilliant Blue R250 (CBB). The levels of G-actin were revealed by Western blot analysis (WB). The relative

densitometry values compared to F-actin are presented (lower panel). B: *N*-acetyl cysteine (NAC) suppressed 35 CuB-induced G-actin pool depletion. Cells were pretreated with NAC (10 mM) for 1 h before exposure to CuB (0.1 μM) for the indicated times. Relative densitometry values (lower panels) are shown.

Fig. S3. Immunofluorescence microscopy analysis of actin and tubulin in CuB-treated B16F10 melanoma cells. B16F10 cells were treated with CuB (0.1 μM) for indicated times and then immunostained with anti-β-actin (green) and anti-β-tubulin (red) antibodies. Nuclei (blue) were revealed by Hoechst33342 staining. Colocalization analysis (lower panels) was performed using Intensity Correlation Analysis (ICA) method. Product of the Differences from the Mean (PDM) images and Intensity Correlation Quotient (ICQ) values (lower right panel) are shown. Magnified images of the boxed areas (merged images) are presented in the insets. Scale bars: 10 μm (5 μm in insets).

Fig. S4. CuB induced cofilin–actin rod formation and persistent cofilin dephosphorylation in B16F10 melanoma cells. A: Analysis of cofilin dephosphorylation in CuB-treated B16F10 cells. Cells were incubated with graded doses of CuB (0.1, 1, or 10 μM) for indicated times. Cell lysates were collected and analyzed by Western blotting using specific antibodies. B: Immunofluorescence microscopy analysis of actin and cofilin in CuB-treated B16F10 cells. Cells were treated with 0.1 M CuB or vehicle (control) for 4 h and then immunostained with anti-β-actin (green) and anti-cofilin (red) antibodies. Nuclei (blue) were revealed by Hoechst33342 staining. Colocalization analysis (lower panels) was performed using ICA method. PDM images and ICQ values (lower right panel) are shown. Cofilin rods were colocalized with actin rods (yellow) in the cells treated with CuB. Scale bars: 10 μm.

Fig. S5. Analysis of ROS levels in CuB-treated A375 cells. A: A375 cells were stained with H 2 DCF-DA (10 μM) for 30 min, and then treated the cells with CuB (0.1 or 1 μM) for 30 min. ROS level in cells was analyzed using flow cytometry. B: A375 cells were stained with H 2 DCF-DA (10 μM) for 30 min, and then treated the cells with CuB (0.1 μM) for 30 min. ROS level in cells was analyzed using fluorescence microscopy. Scale bar: 20 μm.